Forest Ecology and Management 461 (2020) 117948

Contents lists available at ScienceDirect

Forest Ecology and Management

journal homepage: www.elsevier.com/locate/foreco

Can complementary preferential flow and non-preferential flow domains contribute to soil water supply for rubber plantation?

Xiao-Jin Jiang[a,b,*], Sissou Zakari[a], Junen Wu[a,b], Ashutosh Kumar Singh[a], Chunfeng Chen[a,b], Xiai Zhu[a,b,c], Wanjun Zhang[a,b,c], Wenjie Liu[a,b,*]

[a] CAS Key Laboratory of Tropical Forest Ecology, Xishuangbanna Tropical Botanical Garden, Chinese Academy of Sciences, Menglun, Yunnan 666303, China
[b] Center of Plant Ecology, Core Botanical Gardens, Chinese Academy of Sciences, Menglun, Yunnan 666303, China
[c] University of Chinese Academy of Sciences, Beijing 100049, China

ARTICLE INFO

Keywords:
Soil matrix
Dye tracer
Wetting front
Complementary relationship
Rubber tree

ABSTRACT

Preferential flow has always been hotspot of research regarding soil water flow, biological activity, and carbon and nitrogen dynamics. However, the mechanism of water flow exchange between two adjacent zones (with and without root system) and the pattern of soil water supply for rubber are still unclear. In the present study, we considered two plots experiencing similar farming history: in the first plot we measured soil physical properties and soil volumetric water content (VWC) during rainfall, and the second plot was used to visualise water flow path and to measure root biomass. Besides, a model was developed on preferential flow domain (PFD, matching the root zone) and on non-preferential flow domain (NPFD, matching the remote root zone) to compute differences in soil properties between the PFD and NPFD. The results revealed that the dominant flow type in the PFD was preferential flow and the one in the NPFD was capillary flow. Dye stained area and wetting front rate negatively correlated with bulk density, while they positively correlated to non-capillary porosity and root biomass. Accordingly, PFD showed a quick response to rainfall. Indeed, during the rain, a lateral flow (driven by water gravity and pressure head gradient) predominantly carried water (0.95, 0.27, and 0.44 $cm^3\ cm^{-3}$ for various rainfall events 1, 2, and 3, respectively) from PFD to NPFD. During the soil drainage stage, the lateral flow direction changed, and water (about 0.63, 0.30, and 0.39 $cm^3\ cm^{-3}$ for rainfall events 1, 2, and 3, respectively) flowed from NPFD to PFD. As a result, PFD presented low storage and high flow characteristics compared with NPFD, suggesting this complementary relationship for water interaction between the two domains could be beneficial for rubber plants growth and development.

1. Introduction

Preferential flow is the process by which water moves unevenly through soils via preferred path rather than uniform flow (Beven and Germann, 2013; Allaire et al., 2009). The studies regarding preferential flow have attracted global attention (Hirmas et al., 2018; Alaoui et al., 2011; Chappell, 2010; Lago et al., 2010; Posadas et al., 2009; Clothier et al., 2008; Jarvis, 2007; McClain et al., 2003; Jaynes et al., 2001; Uchida et al., 2001) due to its essential contribution in hydrological and ecological processes at different scales (field, catchment, and regional scales) (Zhu et al., 2019; Lin, 2010; Lin and Zhou, 2008; Flury et al., 1994; Bouma, 1981). As a critical hydrologic cycle of ecohydrological process, preferential flow has substantial impacts on runoff generation, soil water storage, moisture distribution, filter and buffer functions, slope stability, species distribution, and biogeochemical cycling in the tropical zone (Liu et al., 2016, 2014). Indeed, preferential flow paths have higher microbial biomass, different community structures; and nitrogen cycling than the rest of the soil (Bundt et al., 2001a, b). These effects could become more critical in Xishuangbanna, China, where ecological and environmental issues are of concerns because of the conversion of natural forests to rubber plantations (Snoeck et al., 2013; Li et al., 2012). Fortunately, these ecological issues can be improved and even restored to a beautiful blueprint through knowledge of the relationship between ecohydrological process and environmental issues (Chen et al., 2018, 2017; Liu et al., 2015, 2014).

The understanding and perspective of preferential flow can vary at different scales and different standard of classification. The preferential flow (resulting from diameter > 2 mm macropore, detected by CT

* Corresponding authors at: CAS Key Laboratory of Tropical Forest Ecology, Xishuangbanna Tropical Botanical Garden, Chinese Academy of Sciences, Menglun, Yunnan 666303, China.

E-mail addresses: jiangxiaojinlinda@163.com (X.-J. Jiang), lwj@xtbg.org.cn (W. Liu).

https://doi.org/10.1016/j.foreco.2020.117948
Received 13 October 2019; Received in revised form 21 January 2020; Accepted 27 January 2020
Available online 05 February 2020

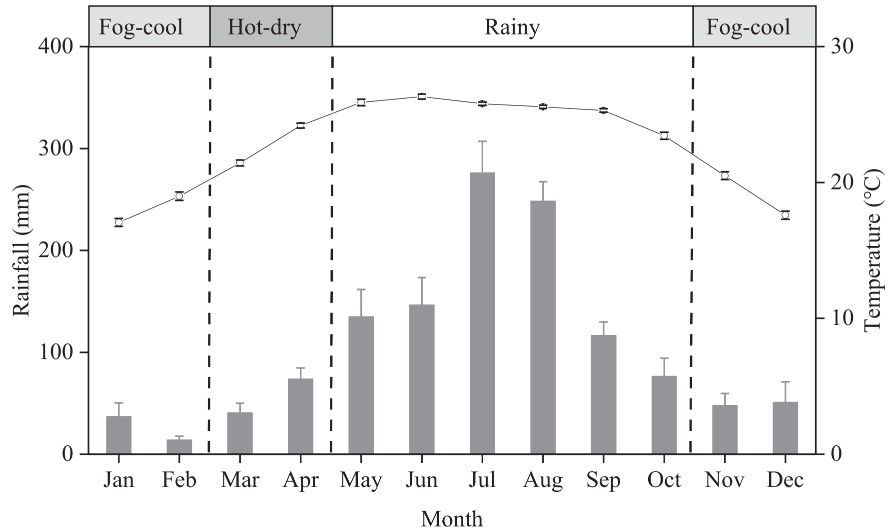

Fig. 1. Month wise precipitation and monthly mean, maximum, and minimum temperatures during the study period (2009–2018). Weather data are provided by the Xishuangbanna Station for Tropical Rainforest Ecosystem that is adjacent to the study site.

scanning) can be observed at soil column (small scale), which might be regarded as matrix flow occurring at field (large scale) when the surface soil section is uniformly stained by dye tracer based on classifying method (Weiler and Flühler, 2004). As a common and effective method, dye tracer has been used to successfully trace water flow and to differentiate the flow paths in soil (Flury and Flühler, 1995; Ghodrati and Jury, 1990). Nevertheless, this method usually relies on a single test, and the patterns of continuous soil water flow during rainfall events could become difficult to illustrate. Fortunately, the spatio-temporal characteristics of preferential flow in response to large storms have been successfully interpreted with a soil moisture sensor network (Wiekenkamp et al., 2016; Liu and Lin, 2015). Thus, the accurate interpretation of water flow behaviours (e.g., matrix flow, preferential flow, lateral flow) can be helpful to understand rainwater redistribution (rainfall infiltration, surface runoff, groundwater recharge, and plant water storage) (Jiang et al., 2019, 2018; Lipiec et al., 2006). Besides, capillary flow is typical to high clay soil (Jiang et al., 2018), which could directly supply water to plants. However, previous studies have been limited to point scales analysis (Jiang et al., 2019, 2018, 2017), and the spatial patterns of soil properties and water variation concerning the specialised root zone of rubber tree remain poorly understood.

The root distribution zone has always been seen as hotspots of research on soil physical, chemical and microbial properties (Bastian et al., 2009; Hinsinger et al., 2009; Luster et al., 2009; Poll et al., 2008). For instance, the root zone is full of large amounts of carbon and nitrogen releasing by dead roots (Bastian et al., 2009). However, soil non-capillary porosity and saturated water-holding capacity are lower in non-root zone than in root zone (Jiang et al., 2019), and soil water flow types (matrix flow, preferential flow, lateral flow), its hydrological properties (field capacity, saturated water-holding capacity), and physical properties (bulk density, non-capillary porosity, particle distribution) can substantially be different between non-root and root zones (Niemeyer et al., 2014; Ludwig et al., 2005). Different water flow behaviours in soil with various root distribution was interpreted by HYDRUS-3D (Jiang et al., 2019). However, the monitoring data in field was more valuable. Therefore, it would be essential to monitor, quantify and analyse the real patterns of soil water content response to rainfall events and soil properties.

Our specific objectives were: (1) to reveal the spatial patterns of soil properties in two different flow domains (PFD and NPFD) under a rubber monoculture and (2) to discriminate water flow paths in the two flow domains using dye tracer infiltration experiments and reveal the spatiotemporal characteristics of soil VWC. Then, (3) we will detect the relationship between soil physical properties (bulk density, non-capillary porosity, total porosity, root biomass) and soil hydrological properties (field capacity, saturated water-holding capacity, capillary water-holding capacity, wetting front rate). Besides, based on the concept of the dual-permeability, we extended the study scale and developed a model assuming that: (1) root zone and adjacent non-root zone match the PFD and the NPFD, respectively; (2) low storage and high flow could characterize the PFD while opposite properties described the NPFD; and (3) a mutual dependence of the two domains for water distribution at saturation and draining stages would rely on water flow behaviour. The results of this research are expected to provide a baseline for foresters and local governments; and will help them to make rational decisions on the water requirement of rubber trees in the study zone and elsewhere in the tropics.

2. Materials and methods

2.1. Experimental site

The study site was located in the Xishuangbanna Tropical Botanical Garden (XTBG; 21°55′39″ N, 101°15′55″ E; 750 m asl), Mengla County, China. The local climate of XTBG is dominated by the southern tropical monsoons from the Indian Ocean during the rainy season (from May to October), and controlled at its southern edges by the subtropical jet streams that prevailed and delivered dry hot and cold air during the dry season (from November to February). The rainfall amount in the region is over 80% of the total annual rainfall during the rainy season (Fig. 1). The soil is classified as loam texture (42% sand, 34% silt and 24% clay) according to USDA-SCS (1994). Rubber plantations are dominant in the XTBG, with *Hevea brasiliensis* trees arranged 2 m apart in double rows set 3 m apart, and each set of double rows separated by a gap of 18 m width. Other crops (e.g., *Citrus reticulate*, *Coffea arabica Linn.*, *Theobroma cacao Linn.*, *Clerodendranthus spicatus*, *Amomum villosum*, *Camellia sinensis*) are intercropped in the gaps between rubber tree rows.

2.2. Soil properties and volumetric water content

Two plots (6.0 m × 6.0 m, 12.0 m distance from each other) were settled in the same planting zone (Fig. 2) containing similar rubber trees (20 years old, height 12.5 ± 1.48 m, stem diameter

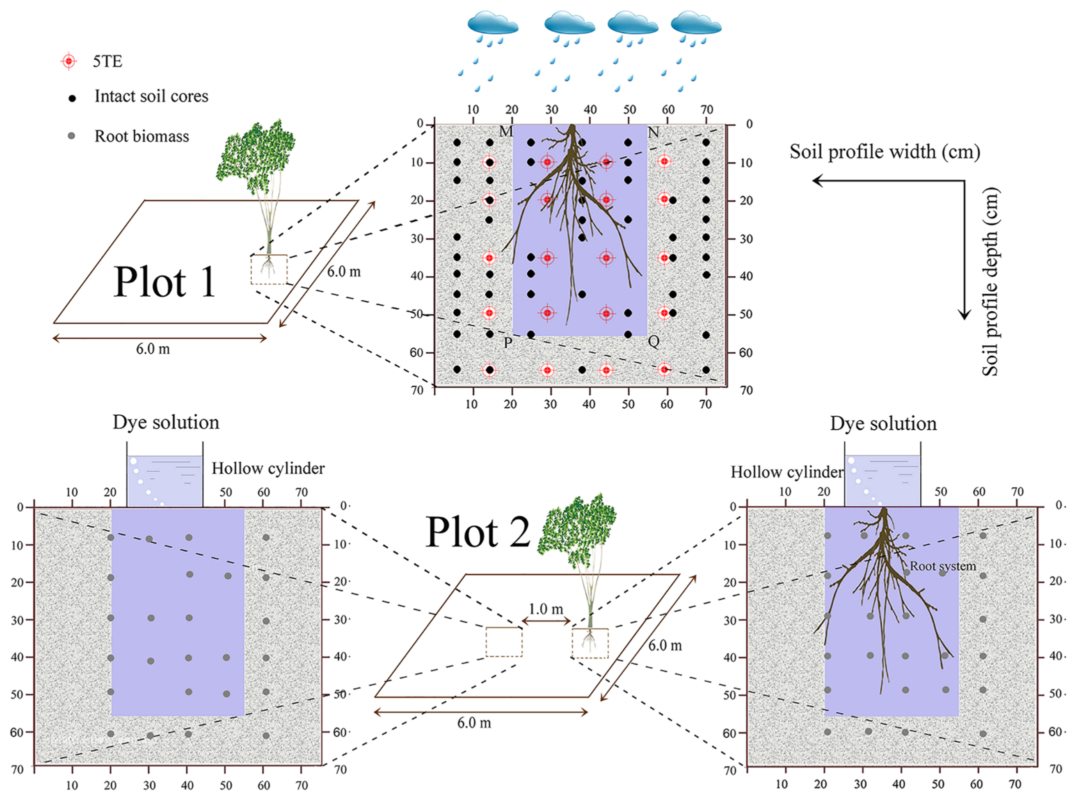

Fig. 2. Diagram of the experimental design. Soil intact sores and 5TE in plot 1, Dye tracer infiltration test and root biomass samples in plot 2. The two plots (1 and 2) were settled at locations where the rubber trees has similar morphological characteristics (20 years old, height 12.5 ± 1.48 m, stem diameter 45.52 ± 1.76 cm), the similar soil condition was assumed for the two plots. The assumed rubber trees root systems were drawn in the soil profiles. The four points (M, N, P, and Q) were divided into the PFD (marking as lilac area) because the four points were covered by wetting front at 30 mins after the rain, and the remaining part of area was supposed as NPFD.

45.52 ± 1.76 cm). In the first plot, we dug a soil pit to prepared a vertical soil profile (70.0 cm depth, 75.0 cm width) (10 cm to the root axis) and used a rubber hammer to drive the volumetric ring (inner diameter, 70.00 mm; height, 52.00 mm; and volume, 200 cm^3) into the vertical soil profile. We further used a sharp knife to cut off the soil around the volumetric ring and also cut off the soil which connected to the vertical soil profile to produce an intact soil core. All the volumetric rings containing wet soil (fifty-three intact soil cores) were carefully transported to the laboratory to determine the soil physical properties (Danielson and Sutherland, 1986). The weights of the empty volumetric ring and the volumetric ring containing wet soil were first recorded as W_{HCR} and W_{CRWS}, respectively; then, the samples were placed in a tray (70.0 cm length, 40.0 cm width, 10.0 cm depth) containing distilled water for the effective saturation experiment in laboratory. The water level in the tray was near the topsoil surface of the volumetric rings, without entering the samples by the top. The weight of soil samples at saturation (W_{SAT}) was measured after ponding the soil core cylinders for 24 h. Afterwards, the saturated soil core cylinders were placed on sand to facilitate their drainage through gravity, then weighted two hours (W_{WD2H}) and five days (W_{WD5D}) after drainage. Finally, the volumetric ring containing dry soil was oven dried at 105 °C for 24 h and weighted (W_{CRDS}); and the total porosity was calculated on the assumption that air was not trapped in the soil pores, then validated using dry bulk density and a particle density of 2.65 g cm^{-3} (Danielson and Sutherland, 1986). The soil properties such as bulk density, non-capillary porosity, total porosity, field capacity, saturated water-holding capacity, and capillary water-holding capacity were determined according to equations given in Zhu et al. (2019).

After the intact soil cores collection, the soil holes were filled with soil from neighbours' similar land to form a flat on soil vertical profile. Then twenty 5TE sensors (Decagon Devices, Pullman, WA, USA) were inserted entirely in the vertical soil profiles of the first plot (0.20 m to rubber tree). The 5TE sensors (10.0 cm length, 3.7 cm width, 0.7 cm thickness) have three prongs to enable simultaneous measurement of subsoil temperature, VWC, and bulk electrical conductivity in soil (Rosenbaum et al., 2010). These data were collected at an interval of 5 mins by the ECH2O Utility software (Decagon Devices, Inc©, Pullman, WA) through an Em50 data logger. After the installation of the 5TE sensors, the soil pit was carefully refilled to form a flat horizontal soil surface. The impact of the sensor installation on water flow and soil properties almost disappeared after four months, during which several rainfall events saturated the soil and the data measured by 5TE became stable, then the 5TE resume to forma work. The VWC was measured during a rainfall event, with an average intensity of 4.8 mm min^{-1}.

2.3. Water flow path interpretation

Dye solution was placed on two quadrats of the second plot for water infiltration experiments. The first quadrat (0.20 m to the rubber tree) was used to track water flow in the PFD, and the second (1.00 m to the rubber tree) was utilized to trace the water flow in the NPFD. In each quadrat, one hollow stainless-steel cylinder (diameter, 0.4 m; height, 0.3 m) was inserted into soil at a depth of 0.05 m. Then, each cylinder was filled with Brilliant Blue FCF dye tracer solution at a concentration of 4.0 g L^{-1} (Flury and Flühler, 1995). Moreover, each cylinder was rapidly refilled to 10 cm height during the infiltration experiments to maintain a constant head (Zhu et al., 2019). The cumulative infiltration volume was 26 L for each quadrat, and the infiltration experiments took 1.5 h for the first quadrat and 84.5 h for the second quadrat.

The soils of two quadrats were dug 24 h after the end of infiltration experiments to obtain two vertical soil sections at the mid-axis of each

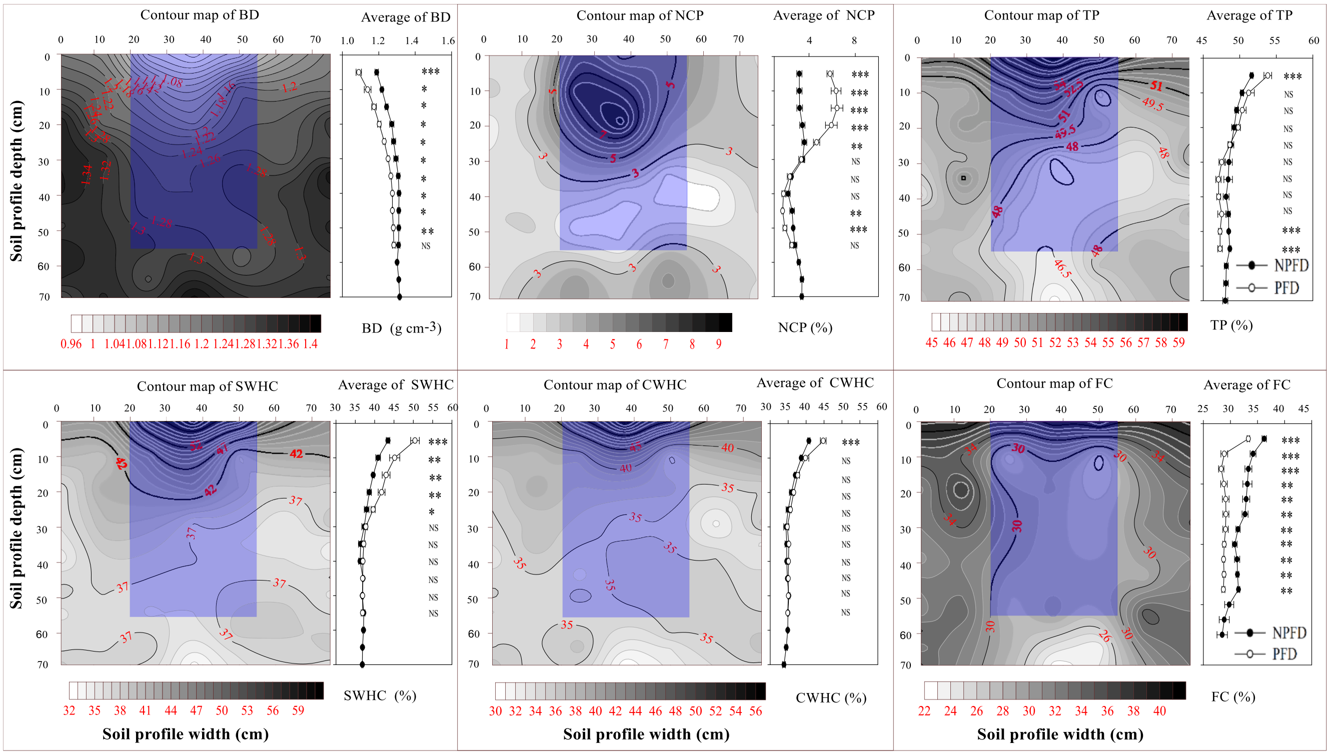

Fig. 3. Spatial distribution contour maps of soil properties in vertical soil profiles and the *t*-test results of their comparisons between the two domains (preferential flow domain and non-preferential flow domain, PFD and NPFD, respectively). BD, bulk density; NCP, non-capillary porosity; TP, total porosity. SWHC, saturated water-holding capacity; CWHC, capillary water-holding capacity; FC, field capacity. * $P < 0.05$. ** $P < 0.01$. *** $P < 0.001$. NS: No significant.

cylinder. The soil sections were photographed using a digital camera (Canon EOS Rebel T3, Japan). For the belowground biomass (Fig. 2), soil samples were collected from each plot down to a depth of 0.6 m using a root sampler (50 mm inner diameter; 50 mm height) (Fig. 2). A total of 50 soil samples were taken to estimate root biomass, and the soil was sieved through a 2-mm mesh, then wash-off to collect the soil roots which were oven dried at 80 °C to a constant weight.

2.4. Spatial interpolation and preferential flow domain classification

Subsequent to soil hydrological features (field capacity, saturated water-holding capacity, and capillary water-holding capacity) and VWC, ordinary kriging in Surfer program (Version 10.0, Golden Software Inc., Golden, CO, USA) was used to produce kriging maps of the VWC, soil physical properties and hydrological properties across the vertical soil profiles. A point (x, y) on the vertical soil section was classified into the PFD if it is covered by the wetting front at a certain period during the rain. For instance, points M (20, 0) and N (55, 0) were classified into the PFD at 15 mins after the beginning of the rain, and points P (20, 55) and Q (55, 55) were divided into the PFD at 30 mins after the rain. Then, the rectangle (35.0 cm width, 55.0 cm depth) formed by the four points (M, N, P, and Q) was assumed as PFD, and the remaining part of the area was supposed as NPFD (Fig. 2). Besides, the lateral flow of the wetting front in the vertical soil section was also recorded at two different times (15 and 30 mins after the beginning of the rain) to determine the wetting front rate of the downward flow; then the wetting front rate and contour between the NPFD and PFD were compared for the rainfall event.

2.5. Statistical analysis

The simulated soil physical and hydrological properties were obtained from the kriging maps. Spearman's correlation was used to establish the relationship between measured and simulated soil properties. The difference in soil properties among NPFD and PFD was analyzed using *t*-test in SPSS 20.0 (Statistical Package for the Social Sciences, USA). All the data were first tested for normal distribution. A log-transformation or square root transformation was applied for non-normally distributed data. Differences were considered significant at $p < 0.05$. A linear redundancy analysis (RDA) was also performed to explore the relationships between soil hydrological and soil physical properties, and a Monte Carlo permutation test was conducted based on

Table 1
Correlation coefficients of soil physical properties between field measurement (FM) and interpolation method (IM). BD, bulk density; NCP, non-capillary porosity; TP, total porosity. Soil hydrological properties refer to FC, field capacity; SWHC, saturated water-holding capacity; CWHC, capillary water-holding capacity.

IM	FM											
	PFD						NPFD					
	BD	NCP	TP	SWHC	CWHC	FC	BD	NCP	TP	SWHC	CWHC	FC
PFD/NPFD	0.895**	0.681*	0.790**	0.909**	0.960**	0.679*	0.905**	0.734*	0.828**	0.862**	0.903**	0.938**

* $P < 0.05$.
** $P < 0.01$.

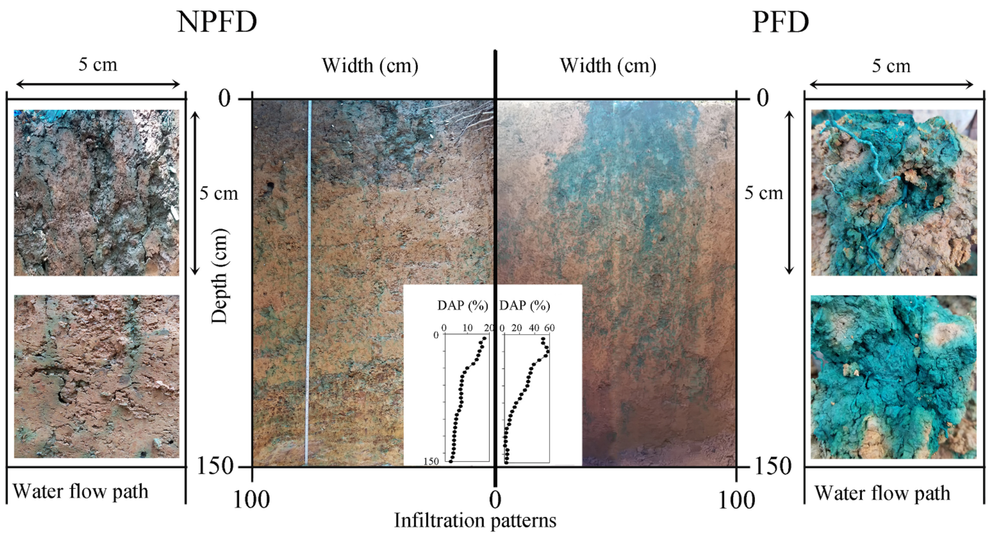

Fig. 4. Different water flow paths and infiltration patterns in non-preferential flow domain (NPFD) and preferential flow domain (PFD), respectively. DAP, Dye area percentage.

499 random permutations to test the significance of the eigenvalues of the canonical axes in CANOCO 4.5 (ter Braak and Smilauer, 2002).

3. Results

3.1. Soil properties distribution patterns

The spatial distribution contour maps showed different soil properties between the two domains (PFD and NPFD) within soil profile (Fig. 3). Because of the different number of measured data that challenged statistical analyses, we instead used the simulated data to compare the soil properties between PFD and NPFD based on the observed strong and significant correlation between measured soil property and its corresponding simulated data (Tables 1). The bulk density was significantly higher in the NPFD than in the PFD from the soil surface to the soil depth of 50 cm ($P < 0.05$). The non-capillary porosity was higher in the PFD than in the NPFD from the soil surface to 25 cm depth ($P < 0.01$), and lower from 45 cm to 50 cm depth ($P < 0.01$). The total porosity was higher in the PFD than in the NPFD at the soil surface ($P < 0.001$), and lower at 50 cm to 55 cm depth ($P < 0.001$). The saturated water-holding capacity was higher in the PFD than in the NPFD from the soil surface to the soil depth of 25 cm ($P < 0.05$). The capillary water-holding capacity was higher in the PFD than in the NPFD at the soil surface, and the field capacity was lower in the PFD than in the NPFD from soil surface to depth of 55 cm ($P < 0.01$). The total root biomass was 6 fold lower in the NPFD than that in the PFD ($P < 0.001$).

3.2. Water flow behaviours and spatiotemporal distribution of volumetric water content

The current study also showed different water infiltration patterns and water flow paths between NPFD and PFD domains (Fig. 4). The dye stained area decreased with the greater depth, and exhibited scattered points with micropores as dominant water flow paths in NPFD; whereas more than half of the dye stained area was confined to the upper 50 cm of soil profile in PFD, with roots and macropores as dominant water flow paths. The temporal distribution of VWC inferred a quick response

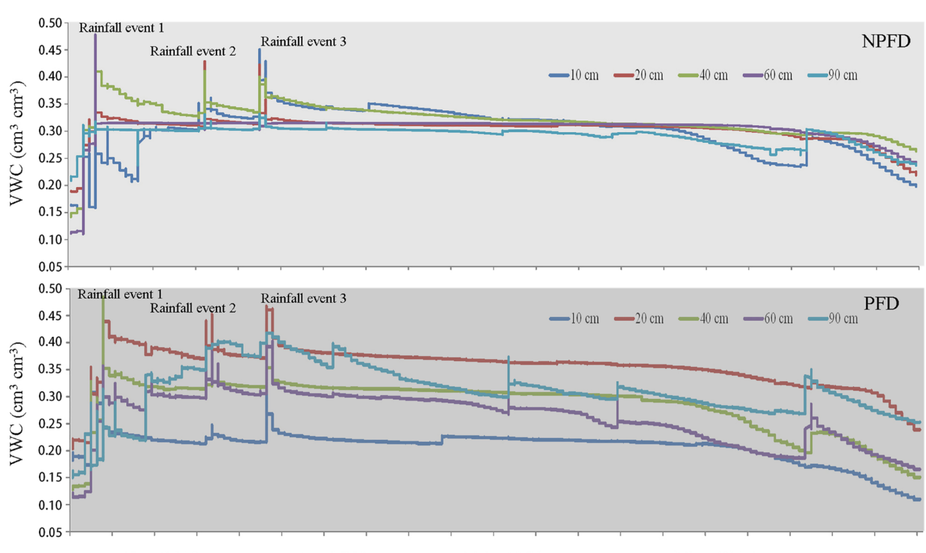

Fig. 5. Volumetric water content (VWC) at different soil depths as a function of rainfall events. NPFD, non-preferential flow domain; PFD, preferential flow domain. Data expressed as an average value of two replications (5TEs) from one soil depth.

Table 2
Descriptive statistics of volumetric water content ($cm^3\ cm^{-3}$) (mean ± SE, n = 40203) in the two domains at various soil depths. PFD, preferential flow domain; NPFD, non-preferential flow domain; SE, standard error of mean; SD, standard deviation; CV, coefficient of variation.

Depth (cm)	Domain	Mean	Maximum	Minimum	SE	SD	CV (%)	Skewness	Kurtosis
10	NPFD	29.90	45.12	15.56	4.58	20.96	70.09	−0.78	0.34
	PFD	20.89	48.05	10.88	3.00	9.02	43.20	−0.87	3.21
20	NPFD	30.32	45.63	14.42	2.42	5.86	19.32	−2.84	10.32
	PFD	35.67	53.36	20.36	3.77	14.22	39.86	−1.18	39.86
40	NPFD	32.11	45.72	14.16	3.35	11.23	34.96	−1.82	34.96
	PFD	28.52	48.44	12.59	4.94	24.45	85.71	−1.34	1.05
60	NPFD	30.42	47.80	10.97	2.96	8.74	28.74	−4.88	27.78
	PFD	26.20	53.50	11.34	4.81	23.10	88.17	−0.75	0.16
90	NPFD	29.19	33.17	20.85	1.80	3.24	11.11	−1.90	3.84
	PFD	31.27	47.59	14.93	4.97	24.68	78.91	−0.30	0.60

of PFD to rainfall compared to NPFD, because the topsoil of PFD (0–10 cm) wetted earlier (about 5 min) than NPFD after the beginning of the rain (first rainfall event on December 20th 2018) (Fig. 5). Furthermore, the coefficients of variation of VWC in NPFD was high at the surface soil layer and decreased almost 6 fold with the rising soil depth, while those of PFD mainly increased only 2 fold from the topsoil to the deep soil (Table 2). Consequently, an opposite trend of VWC existed between NPFD and PFD and the temporal variation of VWC was higher in the PFD than in the NPFD.

The spatial distribution contour maps expressed the VWC patterns and wetting front in the PFD and NPFD. The VWC fluctuated between 0.26 $cm^3\ cm^{-3}$ and 0.44 $cm^3\ cm^{-3}$ in PFD, and between 0.28 $cm^3\ cm^{-3}$ and 0.44 $cm^3\ cm^{-3}$ in NPFD, from beginning to end (Fig. 6A–E) of the rain. Before the rain, the area of wetting front of VWC was higher in NPFD (28 to 38%) than in PFD (26 to 28%), although the two domains experienced similar average values (0.29 cm^3 for NPFD and 0.28 $cm^3\ cm^{-3}$ for PFD). The VWC spread as a downward flow of wetting front 15 min after the beginning of the rain, reaching wetting front VWC ranges of 28–40% and 28–32% for NPFD and PFD, respectively (Fig. 6 B). From 15 min to 60 min after the beginning of rain, both NPFD and PFD domains experienced different variations of VWC distribution, due to the higher downward rate of wetting front in the PFD than in the NPFD. For instance, from 15 min to 30 min during the rainfall event, the depth of the wetting front in the PFD increased by 40.8 cm, which was greater than that in the NPFD (only 17.5 cm rise) for the same period. Besides, the largest difference of average VWC between PFD and NPFD occurred at saturation stage (0.40 $cm^3\ cm^{-3}$ in PFD and 0.33 $cm^3\ cm^{-3}$ in NPFD) (Fig. 6 D), and this difference decreased during drainage 240 min after the rain (0.36 $cm^3\ cm^{-3}$ in PFD and 0.34 $cm^3\ cm^{-3}$ in NPFD) (Fig. 6D–F). Therefore, a lateral flow occurred and transported water from PFD to NPFD during saturation stage (0.95, 0.27, and 0.44 $cm^3\ cm^{-3}$ for various rainfall events 1, 2, and 3, respectively, which is calculated as the difference of VWC between the two domains), and inversely from the NPFD to the PFD during drainage stage (about 0.63, 0.30, and 0.39 $cm^3\ cm^{-3}$ for rainfall events 1, 2, and 3, respectively).

3.3. Effect of soil properties on water flow

The soil hydrological properties (SHP) highly correlated with soil

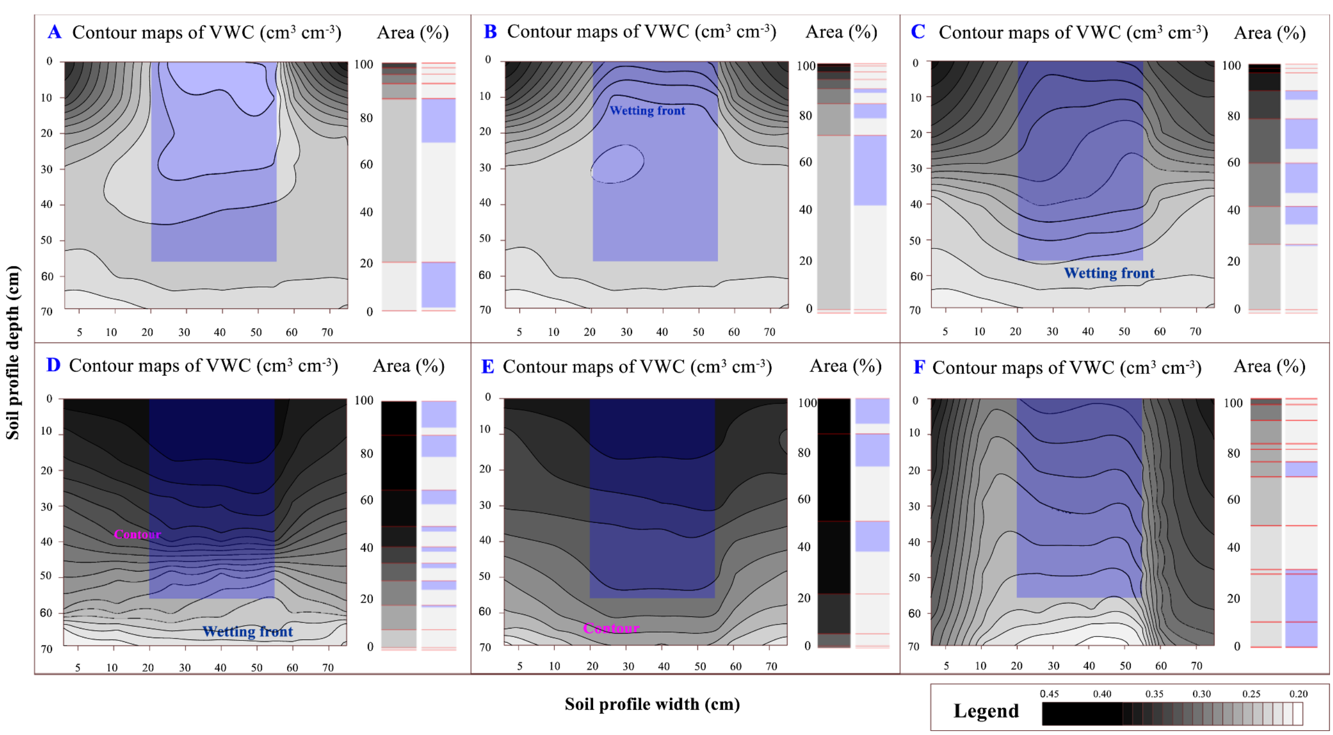

Fig. 6. Spatial distribution contour maps of volumetric water content (VWC) (left) and area (right) in vertical soil profiles. For each area, left side is the percentage area occupied by a specific VWC in soil profile, and right side is the percentage area occupied by a specific VWC in PFD and NPFD. A: before the rainfall; B, C, D, and E: 15, 30, 45, and 60 min after the beginning of the rain, respectively; F: 240 min after the end of the rain. The rectangle (35.0 cm width, 55.0 cm depth) formed by the four points (M, N, P, and Q) was assumed as PFD (marking as lilac area), and the remaining part of area was supposed as NPFD.

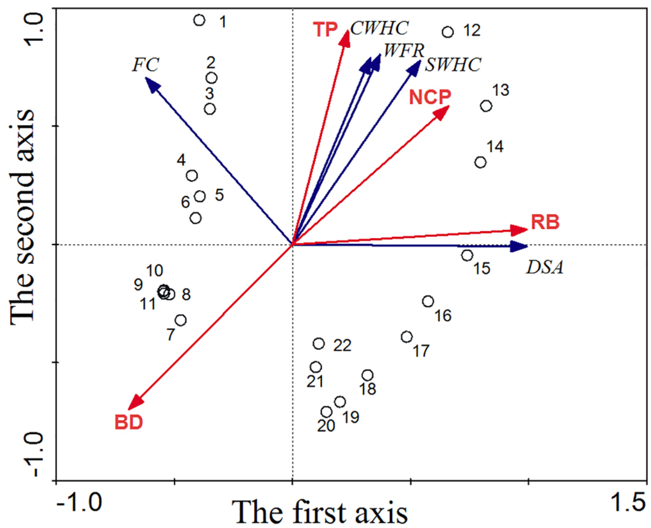

Fig. 7. Ordination diagram showing the results of RDA of soil physical properties and hydrological properties. Soil physical properties refer to BD, bulk density; NCP, non-capillary porosity; TP, total porosity; RB, root biomass. Soil hydrological properties refer to FC, field capacity; SWHC, saturated water-holding capacity; CWHC, capillary water-holding capacity. WFR, wetting front rate. DSA, dye stained area. Soil physical properties and hydrological properties were obtained from the kriging maps. The arabic numbers (1–11 in NPFD; 12–22 in PFD) refer to soil sample number.

physical properties (SPP) as shown the results in the RDA graph (Fig. 7). The RDA results exhibited significant eigenvalues for both canonical axes and first axis (canonical axis: $P = 0.002$ and first axis: $P = 0.002$), and the two RDA axis (SHP the first axis and SPP on second) substantially explained 98% of the total variance in soil properties (Table 3). Root biomass was the dominant SPP, which suitably connected to SHP (first axis), and total porosity was the dominant SPP correlated with the second RDA axis (Fig. 7). Saturated water-holding capacity, field capacity, dye stained area, and wetting front rate negatively associated with bulk density and positively correlated with non-capillary porosity and root biomass. Besides, saturated water-holding capacity, capillary water-holding capacity, and field capacity correlated positively with total porosity, while a negative relationship was noticed between capillary water-holding capacity and root biomass (Fig. 7, Tables 3 and 4).

4. Discussion

4.1. Soil water as affected by soil properties

In the present study, the spatial distribution patterns of soil properties in the vertical soil section exhibited a substantial variation of soil properties between PFD and the NPFD (Fig. 3). The distribution patterns of soil properties mainly matched the root system distribution zone, because of the effects of roots activity and their decomposition on soil properties, and daily disturbance from latex tapping and herbicide application (Zhu et al., 2019). Additionally, the soil physical properties (e.g., bulk density, non-capillary porosity) substantially affected its hydrological properties (e.g., saturated hydraulic conductivity and cumulative infiltration). For instance, bulk density negatively affects saturated water-holding capacity (Chen et al., 2018; Jiang et al., 2018, 2017), which was positively influenced by both non-capillary porosity and total porosity (Table 4 and Fig. 3). Besides, a significant negative correlation existed between bulk density and dye stained area (-0.681, $P < 0.05$) and wetting front rate (-0.769, $P < 0.05$). However, the soil parameters such as root biomass and non-capillary porosity had a substantial positive correlation with dye stained area (0.983, $P < 0.01$ with root biomass and 0.650, $P < 0.01$ with non-capillary porosity) and wetting front rate (0.854, $P < 0.01$ with root biomass and 0.802, $P < 0.01$ with non-capillary porosity) (Table 4). These correlations patterns suggest that the downward water flow was reduced by the high bulk density in NPFD, which was at the same time enhanced by the high root biomass and high non-capillary porosity in PFD. Furthermore, the high porosity resulting from high root biomass in PFD could be beneficial for subsoil water storage during storms. Therefore, more water infiltrated and stored in PFD, then the over-saturated water was delivered to NPFD through paths of preferential flow. As a result, the system PFD-NPFD can reduce the surface runoff and store more water for rubber trees.

Several studies reported that the spatial occurrence of preferential flow mainly depends on soil properties and hydrological conditions (Wiekenkamp et al., 2016; Flury et al., 1994; Ghafoor et al., 2013; Jarvis, 2007). Moreover, the underlying pathways of preferential flow, e.g. root channels, fractures, animal burrows, fissure, crack (Jiang et al., 2019, 2018; Noguchi et al., 2001; Shipitalo and Gibbs, 2000; Bauters et al., 1998; Dekker and Ritsema, 1996; Wang et al., 1996), and their characteristics depend on factors including soil type (Bouma, 1981), tillage management (Andreini and Steenhuis, 1990), and vegetation (Beven and Germann, 2013). Our results suggested that the dominant flow paths in NPFD were micropores, which did not induce an emergence of preferential flow during water infiltration (Fig. 5) because of the high bulk density and low non-capillary porosity of the NPFD (Fig. 3). In contrast, the dominant flow paths in PFD were the interspace and cracks between soil and rubber tree roots, and the soil macropores that derived from the activity and decomposition of root system. These two paths in PFD lead to an occurrence of preferential flow during the rainfall event. Haria et al. (1994) similarly found that cracks and fissures are dominant flow paths in clayey soils. The presence of macropores and the activity and decomposition of roots reduced the soil bulk density while enhancing its non-capillary porosity (Fig. 3). As a result, rubber roots appeared as the most critical factor (being water path as well as affecting soil non-capillary porosity and

Table 3
Results of RDA of soil hydrological properties (SHP) and soil physical properties (SPP). Soil physical properties refer to BD, bulk density; NCP, non-capillary porosity; TP, total porosity; RB, root biomass. Soil hydrologic properties refer to FC, field capacity; SWHC, saturated water-holding capacity; CWHC, capillary water-holding capacity; WFR, wetting front rate; DSA, dye stained area. Soil physical properties and hydrologic properties were from the kriging maps.

Axes	1	2	3	4	Total variance
Eigenvalues	0.798	0.139	0.007	0.050	1.00
SHP-SPP correlations	0.997	0.865	0.807	0.000	
Cumulative percentage variance of SHP data	79.8	93.8	94.9	99.4	
Cumulative percentage variance of SHP-SPP relation	84.6	99.3	100.0	0.0	
Sum of all eigenvalues					1.000
Sum of all canonical eigenvalues					0.944
Test of significance of first canonical axis	Eigenvalue	F-ratio	P-value		
	0.798	71.217	0.002		
Test of significance of all canonical axes	Trace	F-ratio	P-value		
	0.944	101.215	0.002		

Table 4
Correlation coefficients between soil physical properties and soil hydrologic properties. Soil physical properties refer to BD, bulk density; NCP, non-capillary porosity; TP, total porosity; RB, root biomass. Soil hydrologic properties refer to FC, field capacity; SWHC, saturated water-holding capacity; CWHC, capillary water-holding capacity; WFR, wetting front rate; DSA, dye stained area. Soil physical properties and hydrologic properties were from the kriging maps.

Indicator	BD	NCP	TP	RB
FC	−0.969**	0.794**	0.937**	0.612**
SWHC	−0.901**	0.599**	0.933**	0.466*
CWHC	−0.094	−0.071	0.516*	−0.550**
DSA	−0.681*	0.650**	0.226	0.983**
WFR	−0.769*	0.802**	0.583	0.854**

* $P < 0.05$.
** $P < 0.01$.

bulk density) influencing water flow in PFD. Indeed, the dye stained soil exhibited scattered points that distributed from soil surface to 150 cm depth in NPFD (Fig. 4), while the dominant dye stained soil was mostly confined to the upper 50 cm of the soil profile in PFD. In sum, the dominant flow type in PFD was preferential flow which was driven by the action of gravity and pressure head gradient, while NPFD was dominated by capillary flow mainly due to capillary action during the single infiltration test. Finally, the characteristics of these two flow types led to different durations of the dye infiltration with 1.5 h in PFD and 84.5 h in NPFD.

The temporal variation of VWC was higher in PFD than in NPFD as showed the spatial distribution contour maps of VWC (Fig. 5). In fact, the wetting front exhibited a higher downward rate in PFD (2.72 cm min^{-1}) than in NPFD (1.17 cm min^{-1}), which generated a variability of VWC among the two domains. On the other hand, lateral flow occurred during the rainfall as a dominant flow type from PFD to NPFD (Fig. 6). These infiltration patterns compensated the low water content in the NPFD and created a more homogenized water redistribution across the entire soil profile. Indeed, the downward rate of wetting front positively correlated with non-capillary porosity and root biomass (Tables 3 and 4 and Fig. 7). Thus, the area with high range of VWC (0.34–0.45 cm^3 cm^{-3}) increased along with the downward movement of the wetting front (Fig. 6); and the rise was more prominent in PFD than that in NPFD because of differences in bulk density, non-capillary porosity and root biomass between the two domains. Accordingly, the soil layers of PFD wetted earlier by the rain compared with those of NPFD, suggesting PFD had a fast response to rain water than NPFD.

4.2. Characteristics of PFD and NPFD

The PFD and NPFD showed opposite and complementary physical and hydrological soil properties. The PFD was characterized by lower bulk density and field capacity, and higher non-capillary porosity, total porosity, saturated water-holding capacity, and capillary water-holding capacity; while the NPFD was typically with higher bulk density and field capacity, and lower non-capillary porosity, total porosity, saturated water-holding capacity, and capillary water-holding capacity (Fig. 3). This complementarity in soil properties could play an important role in the water infiltration and redistribution process. At the beginning of the rain, if rainfall intensity was higher than infiltration rate, runoff would appear in NPFD. In this case, the deep soil in the PFD could be quickly saturated by this water, especially when the water infiltration rate and its flux in the PFD are higher than those in the NPFD. As a result, lateral flow occurred from PFD to NPFD because of the differences in VWC, wetting front rate and pressure head gradient between the two domains (Fig. 8A). The lateral flow carried water (0.95, 0.27, and 0.44 cm^3 cm^{-3} for various rainfall events 1, 2, and 3, respectively) from the PFD to the NPFD. The lateral flow coexisted with a downward flow, and they extended in the soil profile until saturation (Fig. 8B). Nevertheless, after the rain, water drained faster in PFD than in NPFD due to the higher non-capillary porosity in the PFD, and the lateral flow oppositely occurred from NPFD to PFD at the draining soil zones (Fig. 8C). Then some water (about 0.63, 0.30, and 0.39 cm^3 cm^{-3} for rainfall events 1, 2, and 3, respectively) transported from the NPFD to the PFD. Besides, after the water drainage from soil by gravity and pressure head gradient, more water (high field capacity) first stored in NPFD compared to PFD, then transported to the PFD through capillary force (Fig. 8D). Consequently, the water flow patterns between the two domains played an essential role in water supply mechanism for rubber trees. Another essential characteristic of the two domains was their difference in saturated hydraulic conductivity (K_s), which is a crucial soil parameter used to model water movement and solute transport

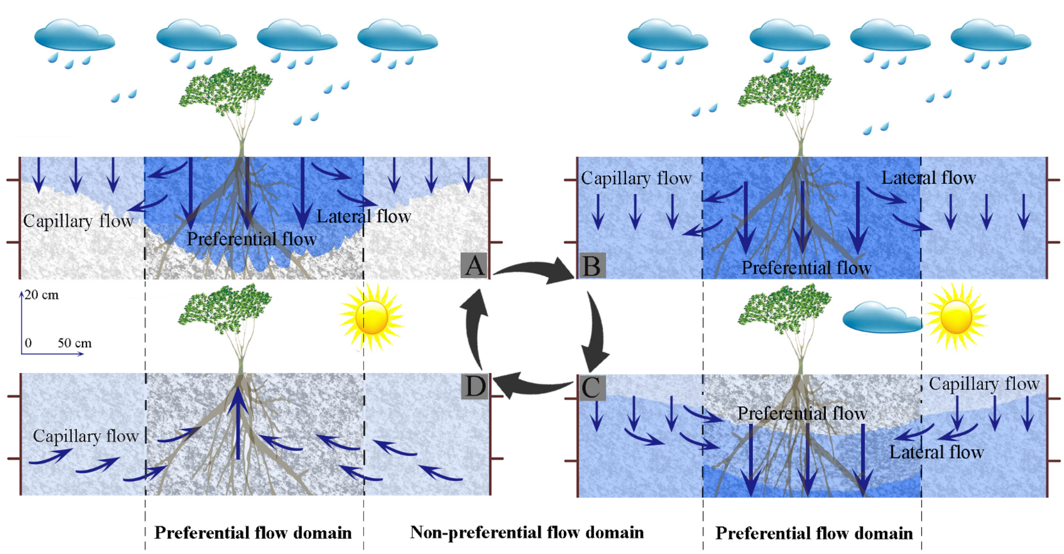

Fig. 8. Conceptual model for soil water dynamic behavior in preferential flow and non-preferential flow domains. A and B: Different strength downward flow and lateral flow were the dominant flow types in the different flow domains at both the beginning of rainfall and the saturation stage. C: Lateral flow occurred from the non-preferential flow domain to the preferential flow domain at soil water draining stage. D: After the water drained by gravity, capillary flow, occurring from the non-preferential flow domain to the preferential flow domain, was the dominant water resource for tea tree.

through soil profile, and expresses the ability of soil to facilitate the water flux under saturated conditions (Kutílek and Nielsen, 1994). Our previously observed K_s values were higher in the root zone than in the no-root zone (Jiang et al., 2019; Niemeyer et al., 2014; Ludwig et al., 2005), resulting in higher K_s in PFD than in NPFD. High K_s and saturated water-holding capacity suggest that a large amount of rainfall water could infiltrate the soil and mitigate surface runoff at the watershed scale. Here, the PFD was typical of low storage and high flow capacities while great storage and low flow capacities inversely characterized the NPFD. Therefore, since the deep roots can affect groundwater recharge (Li et al., 2018), the future researches should also consider roots distribution and their morphological features to precisely classify PFD. This consideration could have valuable implications on understanding ecohydrological processes and water supply mechanisms in natural ecosystems.

The current study revealed the water interaction behaviour of PFD and NPFD domains, as similarly suggest the dual-permeability water flow and solute transport models (Gerke and Köhne, 2004; Vogel et al., 2000). Besides, our findings improved the results of our previous study in which the variation patterns of water flow behaviours in a rubber-based agroforestry system has been interpreted using dye tracer and HYDRUS-2/3D (Jiang et al., 2019). However, our models would be more useful if factors, such as plant root growth, swelling and shrinking behaviour of clays, soil fauna burrows, topographic features, and vegetation cover, were considered for the subsoil hydrological processes modelling.

5. Conclusions

Considering the differences in root distribution, soil properties, and water flow paths between the root zone and its surroundings, we evaluated water flow behaviour in preferential flow domain (PFD, matching the root zone) and non-preferential flow domain (NPFD, matching the remote root zone). The spatio-temporal characteristics of PFD-NPFD system were quantified, and a high resolution soil sampling and water content monitoring were conducted in the field.

The two domains were characterized by inverse soil properties with PFD having low bulk density and field capacity, and high non-capillary porosity and saturated water-holding capacity; while NPFD was of high bulk density and field capacity, and low non-capillary porosity and saturated water-holding capacity. High bulk density weakened the downward water infiltration, which was at the same time enhanced by the high non-capillary porosity and root biomass. Thereby, the wetting front exhibited a higher downward rate in the PFD than in the NPFD. On the other hand, the dominant flow type in PFD was preferential flow with macropores as flow paths, capillary flow dominated in NPFD with micropores as flow paths. PFD exhibited a quick response to rainfall, and the difference in downward rate of the wetting front caused a difference in volumetric water content between the two domains. As a result, a lateral flow appeared from PFD to NPFD during rainfall, and from NPFD to PFD during drainage. These infiltration patterns compensated the insufficiency of soil water for rubber trees, especially during soil water scarcity.

In conclusion, PFD was characterized by small storage capacity and large flow capacity, and NPFD was of large storage capacity and low flow capacity. In a system PFD-NPFD, PFD delivered over-saturated water to NPFD during rainfall while NPFD provided available water (deference between field capacity and wilting coefficient) to PFD for rubber tree. Our findings show that this complementary water interaction relationship between the two domains can be helpful for rubber growth. Our findings also have important implications on the understanding of ecohydrological processes and water supply mechanisms in rubber plantations and natural forests.

Declaration of Competing Interest

The authors declare that they have no known competing financial interests or personal relationships that could have appeared to influence the work reported in this paper.

Acknowledgements

We highly appreciate the valuable comments from two anonymous reviewers, which are very constructive for the improvement of manuscript quality and also provide valuable advices for our further studies. We thank Mr. Liu MN for his help in the fields. We also thank the Central Laboratory of XTBG for their help. This research was supported by the National Natural Science Foundation of China (41701029 and 31570622), China Postdoctoral Science Foundation (2018M633437), the CAS 135-Program (2017XTBG-F01), the Natural Science Foundation of Yunnan Province (2018FB076, 2014HB042), the Natural Science Excellent Youth Foundation of Yunnan Province (2019FI011), and the Youth Innovation Promotion Association CAS (2018430).

Appendix A. Supplementary material

Supplementary data to this article can be found online at https://doi.org/10.1016/j.foreco.2020.117948.

References

Alaoui, A., Caduff, U., Gerke, H.H., Weingartner, R., 2011. Preferential flow effects on infltration and runoff in grassland and forest soils. Vadose Zone J. 10, 367–377.
Allaire, S.E., Roulier, S., Cessna, A.J., 2009. Quantifying preferential flow in soils: A review of different techniques. J. Hydrol. 378, 179–204.
Andreini, M.S., Steenhuis, T.S., 1990. Preferential paths of flow under conventional and conservation tillage. Geoderma 46, 85–102.
Bastian, F., Bouziri, L., Nicolardot, B., Ranjard, L., 2009. Impact of wheat straw decomposition on successional patterns of soil microbial community structure. Soil Biol. Biochem. 41, 262–275.
Bauters, T.W.J., DiCarlo, D.A., Steenhuis, T.S., Parlange, J.-Y., 1998. Preferental flow in water-repellent sands. Soil Sci. Soc. Am. J. 62, 1185–1190.
Beven, K., Germann, P., 2013. Macropores and water flow in soils revisited. Water Resour. Res. 49, 3071–3092.
Bouma, J., 1981. Soil morphology and preferential flow along macropores. Agric. Water Manag. 3, 235–250.
Bundt, M., Widmer, F., Pesaro, M., Zeyer, J., Blaser, P., 2001a. Preferential flow paths: biological 'hot spots' in soils. Soil Biol. Biochem. 33 (6), 729–738.
Bundt, M., Jäggi, M., Blaser, P., Siegwolf, R., Hagedorn, F., 2001b. Carbon and nitrogen dynamics in preferential flow paths and matrix of a forest soil. Soil Sci. Soc. Am. J. 65 (5), 1529–1538.
Chappell, N.A., 2010. Soil pipe distribution and hydrological functioning within the humid tropics: a synthesis. Hydrol. Processes 24, 1567–1581.
Chen, C.F., Liu, W.J., Jiang, X.J., Wu, J.E., 2017. Effects of rubber-based agroforestry systems on soil aggregation and associated soil organic carbon: Implications for land use. Geoderma 299, 13–24.
Chen, C.F., Liu, W.J., Wu, J.N., Jiang, X.J., 2018. Spatio-temporal variations of carbon and nitrogen in biogenic structures of two fungus-growing termites *(M. annandalei* and *O. yunnanensis*) in the Xishuangbanna region. Soil Biol. Biochem. 117, 125–134.
Clothier, B.E., Green, S.R., Deurer, M., 2008. Preferential flow and transport in soil: Progress and prognosis. Eur. J. Soil Sci. 59, 2–13.
Danielson, R.E., Sutherland, P.L., 1986. Porosity. In: Klute, A. (Ed.), Methods of Soil Analysis: Part 1-Physical and Mineralogical Methods. SSSA Book Ser. 5.1. SSSA, ASA, Madison, WI. Pp: 443–461.
Dekker, L.W., Ritsema, C.J., 1996. Preferental flow path in a water repellent clay soil with grass cover. Water Resour. Res. 32, 1239–1249.
Flury, M., Flühler, H., 1995. Tracer characteristics of brilliant blue FCF. Soil Sci. Soc. Am. J. 59 (1), 22–27.
Flury, M., Fluhler, H., Jury, W., Leuenberger, J., 1994. Susceptibility of soils to preferential flow of water: a field study. Water Resour. Res. 30, 1945–1954.
Gerke, H.H., Köhne, J.M., 2004. Dual-permeability modeling of preferential bromide leaching from a tile-drained glacial till agricultural field. J. Hydrol. 289 (1–4), 239–257.
Ghafoor, A., Koestel, J., Larsbo, M., Moeys, J., Jarvis, N., 2013. Soil properties and susceptibility to preferential solute transport in tilled topsoil at the catchment scale. J. Hydrol. 492, 190–199.
Ghodrati, M., Jury, W.A., 1990. A field study using dyes to characterize preferential flow of water. Soil Sci. Soc. Am. J. 54, 1558–1563.
Haria, A.H., Johnson, A.C., Bell, J.P., Batchelor, C.H., 1994. Water movement and isoproturon behaviour in a drained heavy clay soil: 1. Preferential flow processes. J. Hydrol. 163, 203–216.

Hinsinger, P., Bengough, A., Vetterlein, D., Young, I., 2009. Rhizosphere: biophysics, biogeochemistry and ecological relevance. Plant Soil 321, 117–152.

Hirmas, D.R., Giménez, D., Nemes, A., Kerry, R., Brunsell, N.A., Wilson, C.J., 2018. Climate-induced changes in continental-scale soil macroporosity may intensify water cycle. Nature 561, 1002–1103.

Jarvis, N.J., 2007. A review of non-equilibrium water flow and solute transport in soil macropores: principles, controlling factors and consequences for water quality. Eur. J. Soil Sci. 58, 523–546.

Jaynes, D.B., Ahmed, S.I., Kung, K.-J.S., Kanwar, R.S., 2001. Temporal dynamics of preferential flow to a subsurface drain. Soil Sci. Soc. Am. J. 65, 1368–1376.

Jiang, X.J., Chen, C., Zhu, X., Zakari, S., Singh, A.K., Zhang, W., Zeng, H.H., Yuan, Z.-Q., He, C.G., Yu, S.Q., Liu, W.J., 2019. Use of dye infiltration experiments and HYDRUS-3D to interpret preferential flow in soil in a rubber-based agroforestry systems in Xishuangbanna, China. Catena 178, 120–131.

Jiang, X.J., Liu, W.J., Chen, C.F., Liu, J.Q., Yuan, Z.Q., Jin, B.C., Yu, X.Y., 2018. Effects of three morphometric features of roots on soil water flow behavior in three sites in China. Geoderma 320, 161–171.

Jiang, X.J., Liu, W.J., Wu, J.N., Wang, P.Y., Liu, C.G., Yuan, Z.Q., 2017. Land degradation controlled and mitigated by rubber-based agroforestry systems through optimizing soil physical conditions and water supply mechanisms: a case study in Xishuangbanna, China. Land Degrad. Dev. 28 (7), 2277–2289.

Kutílek, M., Nielsen, D.R., 1994. Soil Hydrology. Catena Verlag, Cremlingen, Destedt, Germany.

Lago, M.E., Miralles-Wilhelm, F., Mahmoudi, M., Engel, V., 2010. Numerical modeling of the effects of water flow, sediment transport and vegetation growth on the spatio-temporal patterning of the ridge and slough landscape of the Everglades wetland. Adv. Water Resour. 33, 1268–1278.

Li, H., Si, B., Li, M., 2018. Rooting depth controls potential groundwater recharge on hillslopes. J. Hydrol. 564, 164–174.

Li, H.M., Ma, Y.X., Liu, W.J., Liu, W.J., 2012. Soil changes induced by rubber and tea plantation establishment: comparison with tropical rain forest soil in Xishuangbanna, SW China. Environ. Manage. 50 (5), 837–848.

Lin, H., Zhou, X., 2008. Evidence of subsurface preferential flow using soil hydrologic monitoring in the Shale Hills Catchment. Eur. J. Soil Sci. 59, 34–49.

Lin, H.S., 2010. Linking principles of soil formation and flow regimes. J. Hydrol. 393, 3–19.

Lipiec, J., Kuś, J., Słowińska-Jurkiewicz, A., Nosalewicz, A., 2006. Soil porosity and water infiltration as influenced by tillage methods. Soil Till. Res. 89, 210–220.

Liu, H.P., Lin, H., 2015. Frequency and control of subsurface preferential flow occurrence in the Shale Hills catchment: from pedon to catchment scales. Soil Sci. Soc. Am. J. 79 (2), 362–377.

Liu, W., Zhu, C., Wu, J., Chen, C., 2016. Are rubber-based agroforestry systems effective in controlling rain splash erosion? Catena 147, 16–24.

Liu, W.J., Li, J.T., Lu, H.J., Wang, P.Y., Luo, Q.P., Liu, W.Y., Li, H.M., 2014. Vertical patterns of soil water acquisition by non-native rubber trees (*Hevea brasiliensis*) in Xishuangbanna, southwest China. Ecohydrology 7 (4), 1234–1244.

Liu, W.J., Luo, Q.P., Li, J.T., Wang, P.Y., Lu, H.J., Liu, W.Y., Li, H.M., 2015. The effects of conversion of tropical rainforest to rubber plantation on splash erosion in Xishuangbanna, SW China. Hydrol. Res. 46 (1), 168–174.

Ludwig, J.A., Wilcox, B.P., Breshears, D.D., Tongway, D.J., Imeson, A.C., 2005. Vegetation patches and runoff-erosion as interacting ecohydrological processes in semiarid landscapes. Ecology 86, 288–297.

Luster, J., Göttlein, A., Nowack, B., Sarret, G., 2009. Sampling, defining, characterising and modeling the rhizosphere—the soil science tool box. Plant Soil 321, 457–482.

McClain, M.E., Boyer, E.W., Dent, C.L., Gergel, S.E., Grimm, N.B., Groffman, P.M., Hart, S.C., Harvey, J.W., Johnston, C.A., Mayorga, E., McDowell, W., Pinay, H.G., 2003. Biogeochemical hot spots and hot moments at the interface of terrestrial and aquatic ecosystems. Ecosystems 6, 301–312.

Niemeyer, R.J., Fremier, A.K., Heinse, R., Chávez, W., Declerck, F.A.J., 2014. Woody vegetation increases saturated hydraulic conductivity in dry tropical Nicaragua. Vadose Zone J. 13.

Noguchi, S., Tsuboyama, Y., Sidle, R.C., Hosoda, I., 2001. Subsurface runoff characteristcs from a forest hillslope soil profile including macropores, Hitachi Ohta, Japan. Hydrol. Processes 15, 2131–2149.

Poll, C., Marhan, S., Ingwersen, J., Kandeler, E., 2008. Dynamics of litter carbon turnover and microbial abundance in a rye detritusphere. Soil Biol. Biochem. 40, 1306–1321.

Posadas, A., Quiroz, R., Tanus, A., Crestana, S., Vaz, C.M., 2009. Characterizing water fngering phenomena in soils using magnetic resonance imaging and multifractal theory. Nonlinear Proc. Geoph. 16, 159–168.

Rosenbaum, U., Huisman, J.A., Weuthen, A., Vereecken, H., Bogena, H.R., 2010. Sensor-to-sensor variability of the ECH2O EC-5, TE, and 5TE sensors in dielectric liquids. Vadose Zone J. 9 (1), 181–186.

Shipitalo, M.J., Gibbs, F., 2000. Potental of earthworm burrows to transmit injected animal wastes to tle drains. Soil Sci. Soc. Am. J. 64, 2103–2109.

Snoeck, D., Lacote, R., Kéli, J., Doumbia, A., Chapuset, T., Jagoret, P., Gohet, É., 2013. Association of hevea with other tree crops can be more profitable than hevea monocrop during first 12 years. Ind. Crop. Prod. 43, 578–586.

ter Braak, C.J.F., Smilauer, P., 2002. CANOCO Reference Manual and User's Guide to Canoco for Windows: Software for Canonical Community Ordination (Version 4.5). Micro-Computer Power, Ithaca, NY, US.

Uchida, T., Kosugi, K., Mizuyama, T., 2001. Effects of pipeflow on hydrological process and its relation to landslide: A review of pipeflow studies in forested headwater catchments. Hydrol. Processes 15, 2151–2174.

USDA-SCS, 1994. Key to Soil Taxonomy, sixth ed. Pocahontas Press, Blacksburg, Virginia.

Vogel, T., Gerke, H.H., Zhang, R., van Genuchten, M.Th., 2000. Modeling flow and transport in a two-dimensional dual-permeability system with spatially variable hydraulic properties. J. Hydrol. 238, 78–89.

Wang, D.K., Lowery, B., Norman, J.M., McSweeney, K., 1996. Ant burrow effects on water flow and soil hydraulic propertes of Sparta sand. Soil Till. Res. 37 (2–3), 83–93.

Weiler, M., Flühler, H., 2004. Inferring flow types from dye patterns in macroporous soils. Geoderma 120 (1–2), 137–153.

Wiekenkamp, I., Huisman, J.A., Bogena, H.R., Lin, H.S., Vereecken, H., 2016. Spatial and temporal occurrence of preferential flow in a forested headwater catchment. J. Hydrol. 534, 139–149.

Zhu, X.A., Chen, C.F., Wu, J.E., Yang, J.B., Zhang, W.J., Zou, X., Liu, W.J., Jiang, X.J., 2019. Can intercrops improve soil water infiltrability and preferential flow in rubber-based agroforestry system? Soil Till. Res. 191, 327–339.